,

ASL Environmental Sciences Inc.
#1-6703 Rajpur Place Saanichton, BC
Canada V8M 1Z5 April 2023
TECHNICAL REPORT

The interpretation of multi-frequency acoustic profiling; Part 2: a semi-empirical model of backscatter returns from frazil ice suspensions.

David R. Topham[1] and J.R. Marko
[1]ASL Environmental Sciences Inc., Saanichton, BC, Canada
Correspondence: David R. Topham (dtopham@aslenv.com)

Abstract

A semi-empirical acoustic backscatter model for frazil ice featuring a 2-parameter log-normal distribution of disk shaped frazil ice particles is developed to provide estimates of suspended fractional frazil volume. Fully determined, 3-frequency acoustic equations, provide numerically exact solutions for data subject to a model specific existence criterion. This allows the existence of the exact solutions to be established directly from a data set prior to analysis. Where more than three frequencies are available, inter-comparison of independent 3-frequency solutions provides error bounds on the mismatch between model and data. Examples drawn from both river and marine multi-frequency acoustic data sets are used to provide estimates of mismatch error bounds on frazil fractional volumes of approximately ±25%.

1. Introduction

Multi-frequency acoustic profiling techniques have for several years provided the principal means for estimating fractional ice volumes associated with frazil ice suspended in rivers, (Marko and Jasek, 2010, Jasek et al., 2011, Ghobrial et al., 2013, Marko et al. 2015) and, more recently, in Antarctic ice shelf meltwater plumes (Frazer et al. 2020). In all such cases, a major uncertainty arises from the theoretical representation of the acoustic energy backscattered by suspensions of disk shaped ice particles. A preceding work (Topham and Marko, 2023) designated here as Part 1, establishes general conditions necessary for an algorithm based on a three parameter acoustic backscatter model to extract fully determined solutions from backscatter data acquired at three or more acoustic frequencies. These conditions dictate that ratios of volume backscatter coefficients s_v, measured in pairs of channels sharing a common frequency, satisfy a relationship between corresponding ratios calculated from the utilized theoretical model. The solutions are computationally "exact" in the sense that the search algorithm residuals are vanishingly small, limited only by the numerical precision of the algorithm. Determination of accuracy with respect to the physical properties of the target suspension requires measurements at additional frequencies to provide comparisons of multiple, independent, solutions, representing the same physical acoustic target.

The analytical methods developed showed that the analysis (Marko et al., 2015; Marko and Topham, 2021), based on scattering by elastic spheres (Faran, 1951), did not support exact 3-frequency solutions for Peace River frazil data. This imperfection, a consequence of the thin disk

,

geometry of frazil ice, limited analysis to less informative 2-frquency solutions. The availability of detailed laboratory frazil surrogate data, combined with frazil field data, provided the basis for developing a semi-empirical backscatter cross section model. It is representative of a population randomly oriented, disk-shaped, ice particles of varying aspect ratio, and bridges the gap between the elastic sphere and the elastic cylindrical disk geometry, typical of frazil ice. It will be shown that this relationship provides access to the exact fully determined solutions for data acquired during the Peace River (Marko et al., 2015) and Antarctic (Frazer et al., 2020) study programs.

2. The semi-empirical pseudo-frazil acoustic backscatter relationship

Central to our development is the assumption that a_e, the "effective radius" of an equivalent volume sphere (Ashton, 1983), can be extended to represent the scale length $k_1 a_e$ of a generalized backscatter cross section relationship $\sigma_{BS}(k_1, a_e)$, k_1 being the incident wavenumber. The development draws on two principal sources of information, firstly on the Marko and Topham (2015) laboratory measurements of backscatter cross sections for a family of polystyrene hexagonal disk surrogates, and, secondly, on frazil volume backscatter coefficients derived from Peace River measurements (Marko et al., 2015). Development is initiated by separating the cross-section relationship into a longwave Rayleigh component, and the sum of remaining higher order terms. The Rayleigh contribution utilizes the oblate spheroid (Rayleigh, 1897), with the higher order terms deduced from the laboratory disk measurements. The transposition of results derived from the laboratory measurements to the natural frazil environment draws on computational studies of spherical target models.

To separate the higher order terms, the normalized backscatter cross-section relationship is written in the generic form of Eq. 1, where M and D are the monopole and dipole terms of the Rayleigh solution, and O is the sum of higher order contributions

$$\frac{\sigma_{BS}}{\pi a_e^2} = \left[\frac{(k_1 a_e)^2}{3\sqrt{\pi}} (M+D) - \frac{(k_1 a_e)^2}{3\sqrt{\pi}} O \right]^2 \qquad (1)$$

The higher order terms $(k_1 a_e)^2/(3\sqrt{\pi})O$, can then be expressed in terms of known constituents as,

$$\left(\frac{(k_1 a_e)^2}{3\sqrt{\pi}}\right) O = \left(\frac{\sigma_{BS}}{\pi a_e^2}\right)_{Ry}^{1/2} - \left(\frac{\sigma_{BS}}{\pi a_e^2}\right)^{1/2} \qquad (2)$$

where the subscript *Ry* indicates the Rayleigh solution.

2.1 Laboratory measurements on polystyrene disks and spheres

The availability of 0.125 mm thick, precision-cut hexagonal polystyrene disks, with widths ranging from 0.38 mm. to 6.35 mm, (Marko and Topham, 2015), allowed measurements of backscatter cross sections for populations of identical surrogate targets with dimensions approximating those of frazil ice. A key component of the tests was inclusion of 0.59 mm diameter spherical

,

polystyrene microbeads, equal in volume to the 1 mm width disks. Backscatter measurements were made near-simultaneously at four different frequencies (125, 200, 455, and 769 kHz) in neutrally buoyant brine suspensions. The neutral buoyancy eliminated the dipole term from the longwave Rayleigh contribution, confining the effects of particle geometry to higher order terms.

Complications arose from a shortcoming of polystyrene as a frazil surrogate, in that its characteristic shear wave speed is less than the speed of sound in the host fluid. This allows polystyrene sphere and disk targets to sustain acoustic surface waves which introduce prominent transmission and scattering anomalies (Hay and Schaafsma, 1989; Hefner and Marston, 2000, 2001). These results are excluded from the present investigation, as they are not relevant to ice/freshwater scattering. This restricted the measurements on disk targets to k_1a_e values ≤ 0.58: roughly the lower half of the k_1a_e range typical of frazil measurements. In addition, the 125 kHz measurements for both microbeads, and for disks up to 2.4 mm widths incurred anomalous elevations of roughly 2 dB relative to the theoretical sphere relationship, subsequently traced to sensitivity at this frequency to disturbances generated by manual concentration sampling (Marko and Topham, 2015). For present purposes, these elevated 125 kHz measurements have been excluded.

Input values of the polystyrene shear and longitudinal wave speeds for theoretical calculations were slightly adjusted to optimize the agreement between spherical microbead measurements and corresponding elastic sphere computations. The adjusted wave speeds of 1100 ms^{-1} and 2380 ms^{-1} differed only by 4% and 2% from corresponding speeds calculated by Hay and Schaafsma (1989) from published elastic constants. The spherical target theory then provides a calibrated reference for the disk measurements which accounts for inter-transducer calibration errors. Estimates of backscattering cross sections were derived only from s_V data showing linear dependences on concentration. Complete details of underlying measurements and conclusions are provided in Marko and Topham (2015).

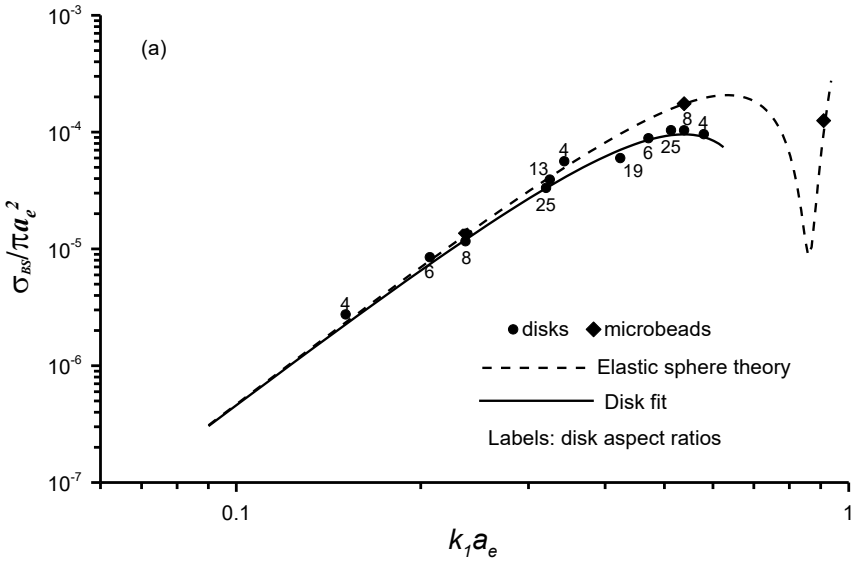

Figure 1a. Summary of single species 1mm polystyrene disks and microbeads, for normalized cross section results a function of k_1a_e. Disk are denoted by circles, microbeads by diamonds.

,

Figure 1a summarizes measured cross section results for disk widths up to 3.18 mm, with individual points labelled with width to thickness aspect ratios, *w*/*t*.

The disk data closely follow the sphere theory up to $k_1a_e \approx 0.3$, followed by a progressively increasing shortfall to about 2.5 dB at the upper disk limit of $k_1a_e = 0.58$. With the exception of a single point of aspect ratio 4 at $k_1a_e = 0.34$, the correlation of the disk results with k_1a_e, irrespective of aspect ratio, supports the extended effective sphere scaling assumption.

Differencing measurements of equal volume 1 mm (aspect ratio 8) disk and spherical microbead suspensions eliminates common errors, including transducer calibrations, and the above-discussed overestimates of 125 kHz cross sections. Subtraction of sphere and disk equations in the form Eq. (1) then allows the higher order terms for the 1mm disk to be extracted from the subtracted measured quantities.

$$\left(\frac{(k_1a_e)^2}{3\sqrt{\pi}}\right)(O_D - O_S) = \left[\left(\frac{\sigma_{BS}}{\pi a_e^2}\right)_S^{1/2} - \left(\frac{\sigma_{BS}}{\pi a_e^2}\right)_D^{1/2}\right]_{measured} \quad (3)$$

where the subscripts *S* and *D* indicate sphere and disk values respectively. The higher order terms of the sphere O_S are derived from computations of the elastic solid sphere theory; the quantities within the square brackets are individual measured values. The disk and sphere measurements are compared in Table 1.

Frequency kHz	k_1a_e	$\sigma_{BS}/\pi a_e^2$ microbead	$\sigma_{bs}/\pi a_e^2$ 1mm disk	$\sigma_{bs}/\pi a_e^2$ Sphere theory	Difference microbead-disk
125	0.148	3.394×10^{-6}	3.213×10^{-6}	2.254×10^{-6}	1.816×10^{-7}
200	0.237	1.365×10^{-5}	1.177×10^{-5}	1.353×10^{-5}	1.878×10^{-6}
455	0.538	1.754×10^{-4}	1.025×10^{-4}	1.767×10^{-4}	7.288×10^{-5}

Table 1. Comparisons between elastic solid sphere theory and measured microbead and 1mm disk backscatter cross sections.

Note the near equality of the 125kHz microbead and 1 mm disk terms, and their elevation. with respect to the theoretical sphere theory; the final column lists their differences.

The higher order disk terms O_D from Eqn. (3) are utilized to calculate the backscatter cross-sections for polystyrene disks from Eqn. (1), and are listed in Table 2.

k_1a_e	$s_{bs}/\pi a_e^2$ Sphere theory	Higher order disk terms	$s_{bs}/\pi a_e^2$ disk
0.148	2.254×10^{-6}	6.094×10^{-5}	2.1065×10^{-6}
0.237	1.353×10^{-5}	4.571×10^{-4}	1.1659×10^{-5}
0.538	1.767×10^{-4}	9.863×10^{-3}	1.0353×10^{-4}

Table 2. Backscatter cross-section and higher order terms for polystyrene disks.

,

The higher order disk terms corresponding to Fig. 1a are shown in Fig 1b. The terms derived from differencing, listed in Table 2, are marked by cross symbols and fitted by the simple power law indicated by the solid line. The circular symbols are the higher order terms calculated directly from Eq. (2), ie. without the error cancelling of the matched volume differencing. With the exception of the low point at k_1a_e below about 0.3, where differences from the sphere theory are negligible, the points closely align with the power law fit of the differenced points. The aspect ratio 4 and 13 points at $k_1a_e = 0.35$, (w = 0.5 mm, 455kHz) correspond to small cross section overestimates. More important is the close correlation of all points above $k_1a_e = 0.4$, as these confirm and extend the power law approximation to the k_1a_e limit of 0.58. The close correlation irrespective of the aspect ratio further confirms of the validity of the extended "effective radius" assumption.

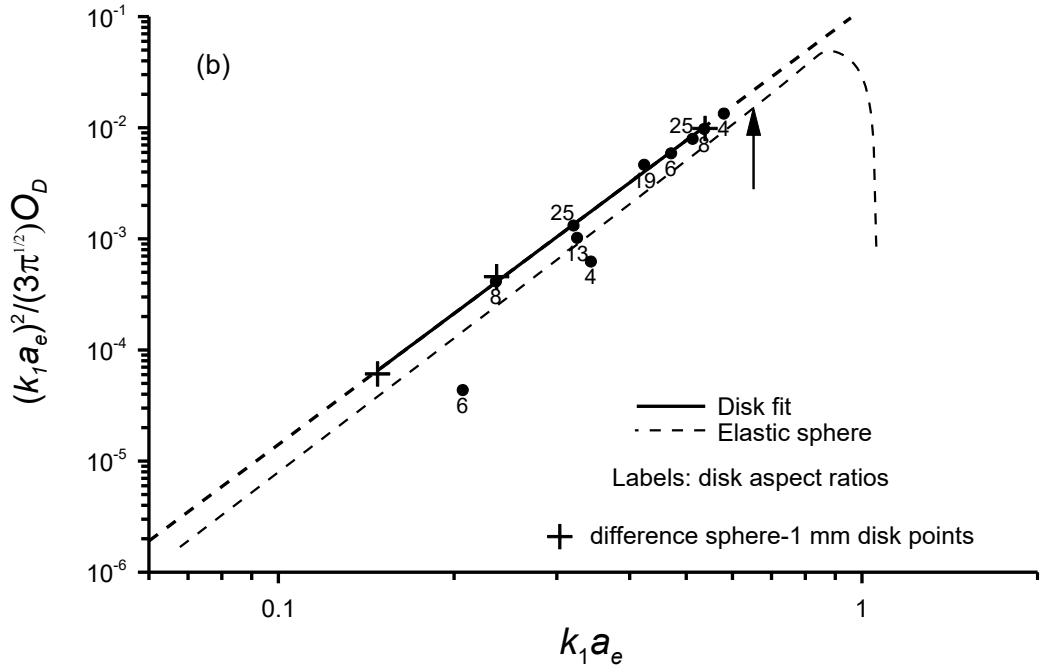

Figure 1b. Higher order terms of polystyrene disks and elastic sphere theory, + differenced measurements, ● individual measurements.

For comparison, the higher order relationship from the elastic sphere theory is also plotted; it follows a similar power law, extending beyond the disks before reaching a maximum at 0.9. The arrow marks the local maximum in the corresponding cross section relationship, which occurs well within the power law region of higher order terms. This suggests the high probability of a similar local maximum in the disk cross section relationship. The final form of the reconstructed disk backscatter cross section relationship, shown as the full line in Fig. 1a, represents a suspension of disks of random orientation and aspect ratio, the latter ranging between 4 and 25, encompassing the anticipated range of river frazil particles.

.

,

2.2. Transposition of polystyrene disk backscatter results into the river frazil environment.

For applications to frazil ice, disk backscatter cross section relationship of Fig. 1a must be translated from the neutrally buoyant brine/polystyrene environment to the weakly positively buoyant freshwater/ice environment. This introduces a negative dipole term into the oblate spheroid Rayleigh solution which is now sensitive to both aspect ratio and orientation. As the incident wave vector becomes aligned with the radial plane of the oblate spheroid, the negative dipole contribution decreases, increasing the total backscattered energy.

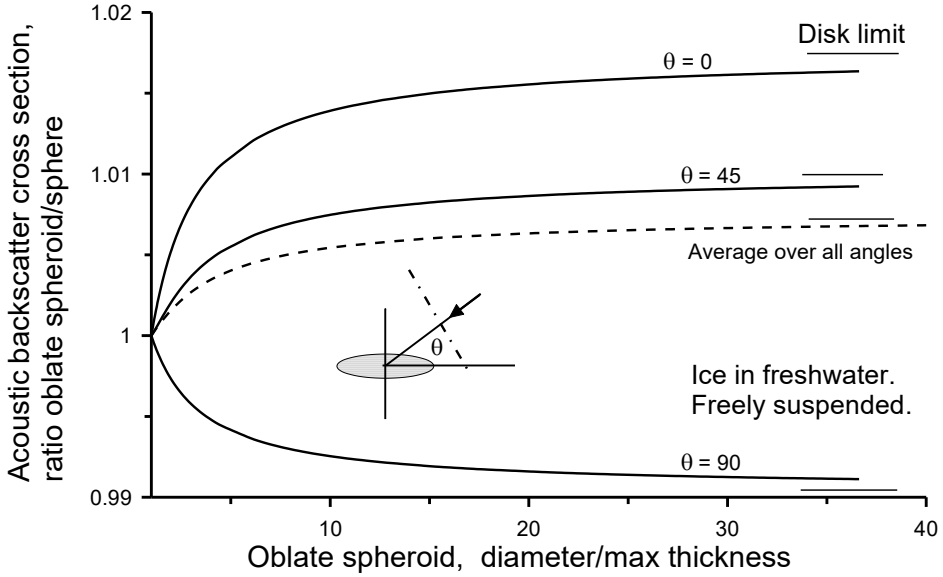

Figure 2. The Rayleigh limit acoustic backscatter cross section as a function of diameter/thickness ratio and orientation for a freely suspended oblate ellipsoid relative to the equivalent volume sphere.

Figure 2 compares the Rayleigh solution for the backscatter cross section of an oblate spheroid of ice suspended in freshwater with corresponding cross sections of an equivalent volume sphere, where the spheroid is progressively transformed at constant volume from a sphere to the thin disk limit. The insensitivity of the scattering strength to both particle shape and orientation is evident, with a maximum range of about 3%. Averaging over all configurations yields an overall mean spheroid/sphere cross section ratio of 1.0036, i.e. the Rayleigh solution for the random oblate spheroid suspension remains that of the equivalent volume sphere.

The transposition of the higher order terms is more problematical and, for guidance, we draw on comparisons of the higher order terms derived from the following spherical scattering models: elastic spheres of polystyrene in brine, ice in freshwater; and for liquid spheres with the sound speed of ice, suspended in freshwater. The normalized theoretical backscatter cross sections, $\sigma_{BS}/\pi a_e^2$, for each of these models are plotted in Fig. 3a as functions of $k_1 a_e$. The elastic sphere cross section curves (A and B) are distinguished by deep local minima in the vicinity of $k_1 a_e = 1$, these minima vary in depth and width reflecting the differences in host fluid and target material properties. Importantly the characters of these curves are distinguished by the ratio of shear wave

,

speeds in the target material to the speed of sound in the host fluid. For polystyrene/brine (A), characterized by the most pronounced minimum, this ratio is less than unity, while for ice/freshwater (C), the ratio exceeds unity, with consequent reduction in the depth of the minimum. The liquid model cannot sustain shear stress and has no minimum. Comparisons with calculations (not shown) for ice spheres in neutral density suspensions showed the effects of small density differences to be largely confined to the dipole term, with negligible effect on the higher order terms. The backscatter characteristic derived from the brine/polystyrene disk suspensions is shown as curve (B),

The corresponding sums of higher order terms deduced from Eq. 2 are plotted in Fig. 3b: with the ordinates of the ice and liquid ice sphere curves being displaced by one and two decades respectively to facilitate visual comparisons. The curves are remarkably similar and obey simple power laws over the relevant range of k_1a_e (bold solid lines). Corresponding parameters are listed in Table 3. For the two elastic sphere models, the higher order power laws extend beyond the local peaks of the cross-section curves. The positions of these peak are indicated by arrows in Fig. 3(b).

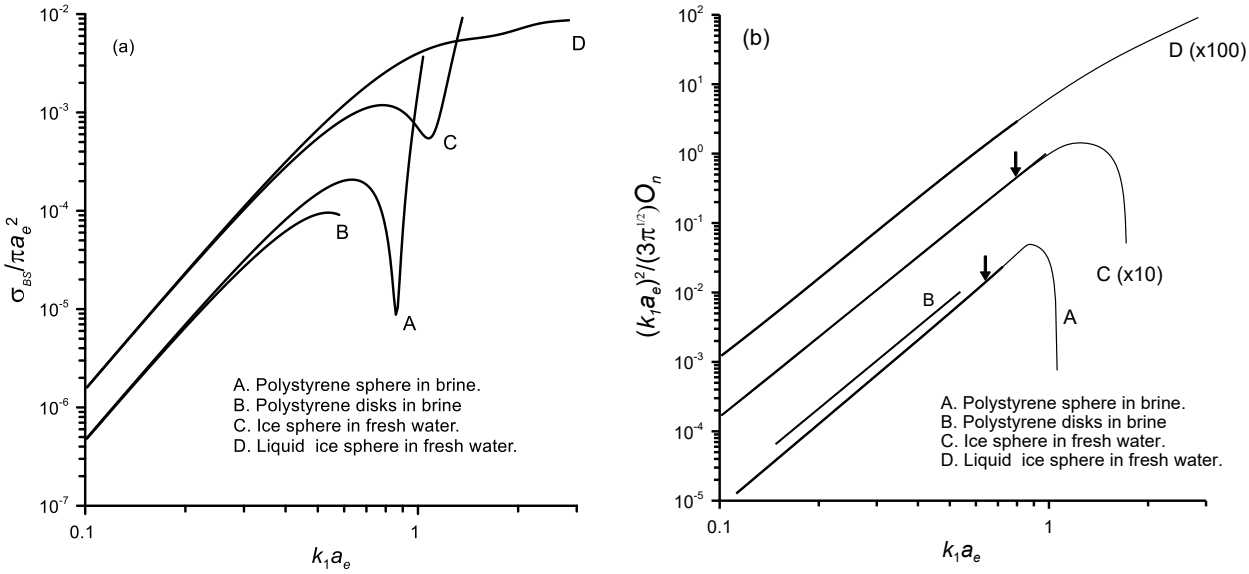

Figure 3. (a) Backscattering cross sections of spherical and disk-shaped polystyrene and spherical ice targets. (b). Higher order terms extracted from the cross sections of (a). Origins of curves C and D are shifted by multiplication by factors of 10 and 100 for clarity: Arrows denote the positions of corresponding peaks in the sphere cross sections of 4 (a).

The major difference between the higher order terms lies in the proportional coefficients of the power law representations and, in lieu of obvious alternatives, it was assumed that the higher order disk terms of natural freshwater frazil bore the same ratio to those of the ice sphere as for the polystyrene/brine system. The parameters of the associated power laws are listed in Table 3 below, the final row listing the values deduced for the transformed frazil ice/freshwater system.

,

Model environment	Coefficient a_0	Power law index m	k_1a_e range	Rayleigh coefficient, R
Polystyrene sphere/brine	0.0836	4.0307	0.11 to 0.9	4.7854×10^{-3}
Elastic ice sphere/water	0.1078	3.8234	0.1 to 1.0	1.5591×10^{-2}
Liquid "ice" sphere/water	0.0710	3.7769	0.1 to 0.8	1.5591×10^{-2}
Polystyrene disk/brine	0.1159	3.9145	0.1 to 0.58	4.7865×10^{-3}
Transformed, ice disk/water	0.1495	3.7131	0.1 to 0.657	1.5591×10^{-2}

Table 3. Power law fits to higher order backscatter terms, $O(k_1a_e)^2/(3\sqrt{\pi})$

The transformed normalized backscatter cross section relationship is henceforth referred to as the "pseudo-frazil" relationship, and is considered to be validated by the laboratory disk measurements to $k_1a_e = 0.6$.

2.3 Bootstrap extrapolation of the pseudo-frazil disk backscatter relationship.

In practice, measurements in natural frazil ice extend beyond $k_1a_e = 1$ and. for practical applications, the "validated" pseudo-frazil cross section derived from the laboratory measurements must be extended to higher k_1a_e values. This extension uses a "bootstrap" technique whereby frazil population parameters derived from within the validated region, allows inversion of data simultaneously acquired in higher frequency channels. The results consist of estimates of σ_{BS} at k_1a_e values beyond the validated regime. Two-channel processing, based on the assumption of a uniform particle distribution, provides estimates of particle number density and equivalent volume radius a_e from within the validated region compatible with single species laboratory data. Field data were selected from 4-frequency Peace River data sets collected during the 2011-12 deployment (Marko et al., 2015). Of the four frequencies (125, 235, 455 and 774 kHz), erratic behaviour of the 235 kHz data limited options to the other three data channels. The March 20 frazil interval, which contained long periods of stable, slowly varying backscatter data, provided a suitable data base for bootstrap extensions.

The long wavelength Rayleigh component of the solution is a known quantity, and the need for empirical extrapolation is thus confined to the higher order terms. The smooth monotonic behaviour over the range of interest, Fig. 3b, provides a relatively robust basis for extrapolation. The extended cross section relationship is then calculated from Eq. (2). A 3rd order polynomial provides interpolation between the validated region and the bootstrap points. A corresponding data set from the highly dynamic Jan 14 frazil interval provided an independent check on the bootstrap values. Figure 4a shows the completed extension of the pseudo-frazil higher order terms. The insert shows a detail of the bootstrap region, with the independent set of Jan 14 points merging smoothly with the March 20 bootstrap points. The extended pseudo-frazil relationship is shown in Fig. 4b, where curve (A) most strongly differs from the sphere (B) over the k_1a_e range between 0.6 and 1.0, a critical operational range for river ice studies, with a maximum reduction of 4 dB at $k_1a_e = 0.8$.

,

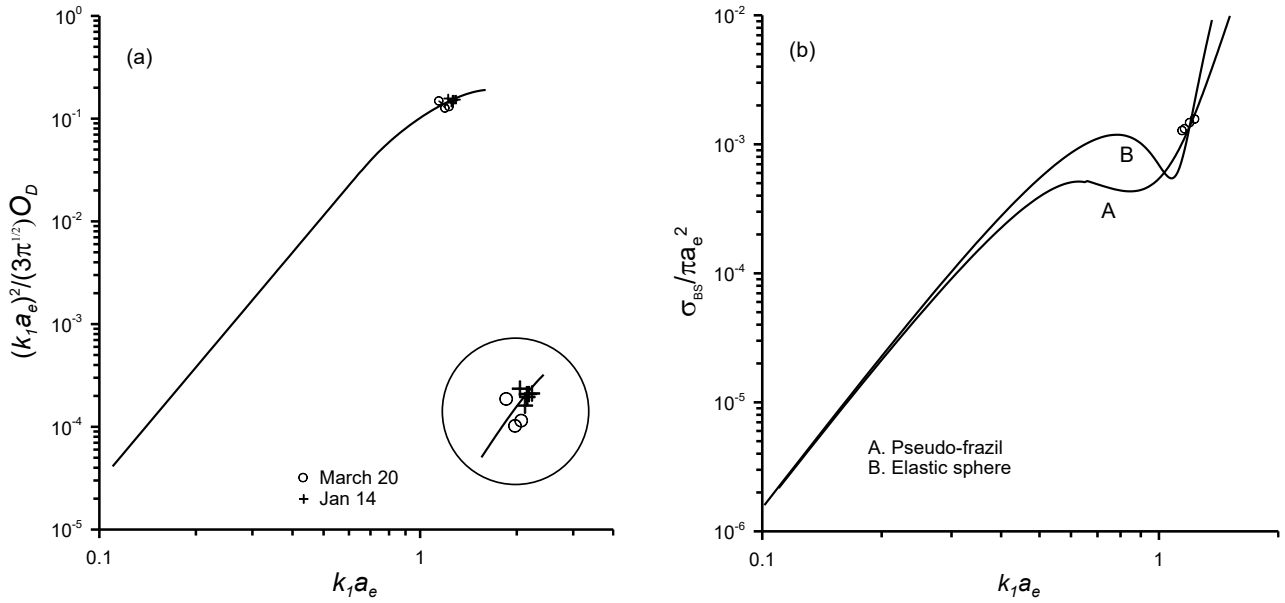

Figure 4. (a) Pseudo-frazil bootstrap extrapolated higher order fit. (b) Normalized backscatter cross sections characteristics of the pseudo-frazil (A), elastic sphere (B), and a randomly oriented liquid 30:1 aspect ratio oblate spheroid (C).

The freshwater pseudo-frazil relationship (A) is given by the following equations:

$$k_1a_e \leq 0.657: \quad \frac{\sigma_{BS}}{\pi {a_e}^2} = \left[{R_y}^{1/2}(k_1a_e)^2 - a_0(k_1a_e)^m\right]^2 \tag{4}$$

$$0.657 < k_1a_e < 1.2: \quad \frac{\sigma_{BS}}{\pi {a_e}^2} = \left[{R_y}^{1/2}(k_1a_e)^2 - (b_0 + b_1(k_1a_e) + b_2(k_1a_e)^2 + b_3(k_1a_e)^3)\right]^2$$

$R_y = 0.015591$, $a_0 = 1.4948$, $m = 3.7131$, $b_0 = 0.005234$, $b_1 = -0.1635$, $b_2 = 0.4022$, $b_3 = -0.1424$.

The extension of the interpolation beyond the bootstrap points is unvalidated.

3.0 The pseudo-frazil backscatter model as a tool for multi-frequency analysis

For application to analysis, the pseudo-frazil relationship has been incorporated in the fully determined lognormal, 3-parameter backscatter model analyzed in Part 1, (Topham and Marko, 2023), (McFarlane, et al., 2017). For access to the fully determined solutions, the acoustic equations are expressed in terms of ratios of volume backscatter coefficients s_{Vi}/s_{Vj} , (Hay and Sheng, 1992), denoted as $G(i,j)$, where i and j specify data channel numbers. This reduces the problem to the solution of a pair of equations in the lognormal distribution parameters a_m, and b, the mean effective radius, and distribution width. A simple least squares routine then suffices to locate the exact solutions, identified by near zero residuals. A particle number density N is calculated for each frequency from a_m and b, together with the three measured backscatter coefficients; the equality of the three values confirms the validity of the solution.

,

To assess the accuracy of the physical output parameters additional frequencies are required to generate alternative, independent solutions; their inter-comparison then provides an appropriate measure of uncertainly. For example, a 4-frequency data set provides six, 2-frequency, and four, 3-frequency fully determined solutions, with the standard deviation of the more accessible 2-frequency solutions providing a robust measure of uncertainty. As a diagnostic tool, the 2-frequency results supply information for specific ranges of the theoretical backscatter cross section relationship, invaluable for model validation.

Two data sets were available for the verification, the three usable frequencies of the 2011-12 Peace River data utilized for the model development, and a complete 4-frequency data set recorded in McMurdo Sound, Antarctica, Frazer et al. (2020). The 3-frequencies of Peace River data were insufficient to define credible uncertainties, and attention therefore is focused on comparisons of frazil volume fraction estimates from 3-frequency pseudo-frazil solutions and the 2-frequency elastic sphere solutions. The 4-frequencies of the McMurdo Sound data provide a full evaluation of the pseudo-frazil algorithm and backscatter model.

3.1 Evaluation of the Peace River multifrequency data

The irregular behaviour of the 200 kHz data channel limited the evaluation to three 2-frequency, and one 3-frequency independent solutions. Evaluation is therefore focussed on the existence of 3-frequency solutions and their relationship to frazil fractional volumes derived from the 2-frequency elastic sphere solutions presented in Part 1 of the current work. Figs 5a and 5b, show solution maps for the March 20 and Jan.14 frazil intervals.

For solutions to exist, corresponding ratios of data points must lie above the lower boundary of the diagram, a condition satisfied by a high proportion of both data sets which are representative of the extremes of 2011-12 winter freeze up conditions. March 20 frazil interval provided, stable slowly changing returns throughout the interval: the Jan 14 interval, a highly dynamic sequence of linked episodes. It is important to note that these maps not only determine the existence of solutions prior to analysis, but also identify the range of particle distribution widths, a feature which provides necessary guidance in selecting data for 2-channel analysis.

,

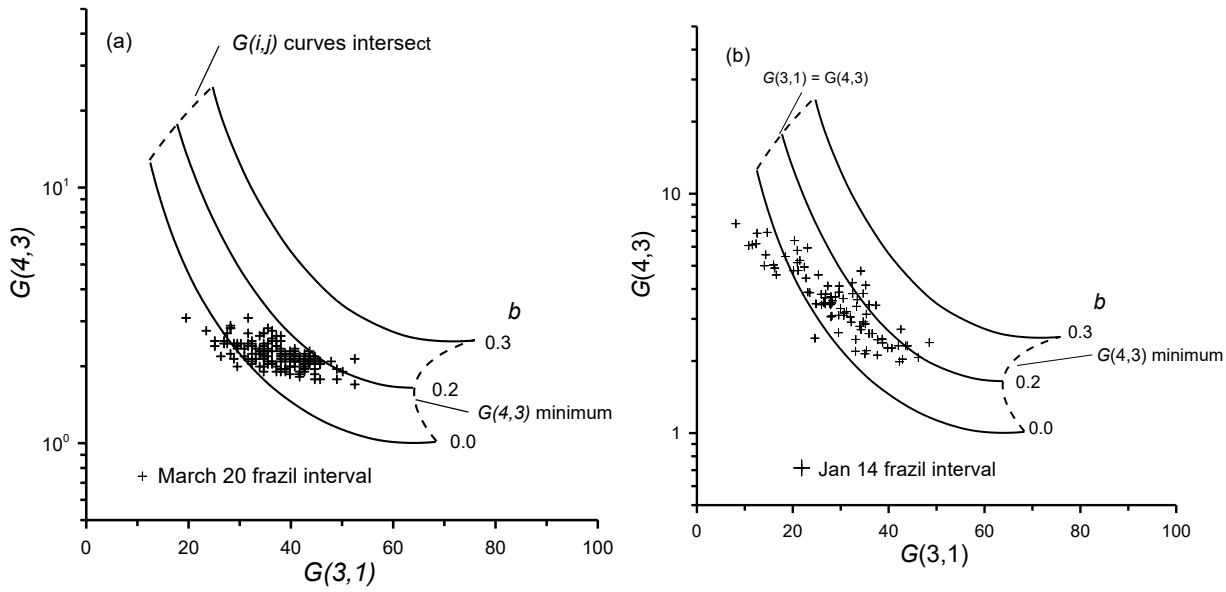

Figure 5. Pseudo-frazil 3-frequency solution diagrams; (a) the March 20 frazil interval, (b) Jan 14.

Figure 6 compares the March 20 frazil interval, 3-frequency pseudo-frazil fractional volumes $F(t)$, with the weighted mean of the three, 2-channel elastic sphere solutions.

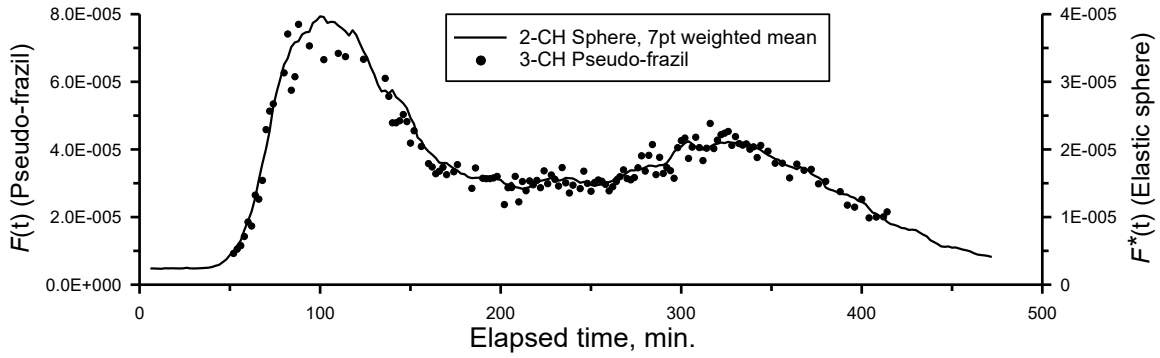

Figure 6. March 20 frazil interval, fractional volume $F($t) at 2.6 m elevation: 3-channel pseudo-frazil model solutions ●; ─ elastic sphere, 7 pt. weighted mean of three, 2-channel combinations, note 2:1 note the difference in vertical scales.

It can be seen that the elastic sphere model consistently underestimates the pseudo-frazil analysis by about 50%, note that the F^*(t) scale for the sphere has been adjusted by a factor of 0.5 for an optimal visual comparison.

,

3.2 Application of the evaluation protocol to a 4-frequency Antarctic data set

An alternative approach to the analysis of acoustic returns from frazil ice based on a liquid oblate spheroid, Kungl et al. (2020), has been applied to data from the McMurdo Sound Antarctic ice shelf plume, Frazer et al. (2020). Data were recorded by upward looking sonar at frequencies of 125, 200, 455 and 769 kHz, almost identical to those of the Peace River data of Section 3.1. This provided an opportunity to evaluate a marine version of the pseudo-frazil algorithm against a comparable 4-frequency data set.

Frazer at al. provide graphical S_V depth profile for 1800 (local time) November 11 2017 and accordingly, a 12 hour period of digital S_V data centred on the depth profile at the 15 mBSL level, was downloaded from Robinson et al. (2020). (times are quoted from Fazer et al. 2020, which appear to be local). Overall, the S_V data were about 20 dB below the peak Peace River values. Figure 7 provides an overview of the selected data set, each point indicating the existence of a 2-frequency solution. The co-existence of at least two, 2-frequency solutions sharing a common frequency, is a prerequisite for the existence of the exact 3-frequency solutions.

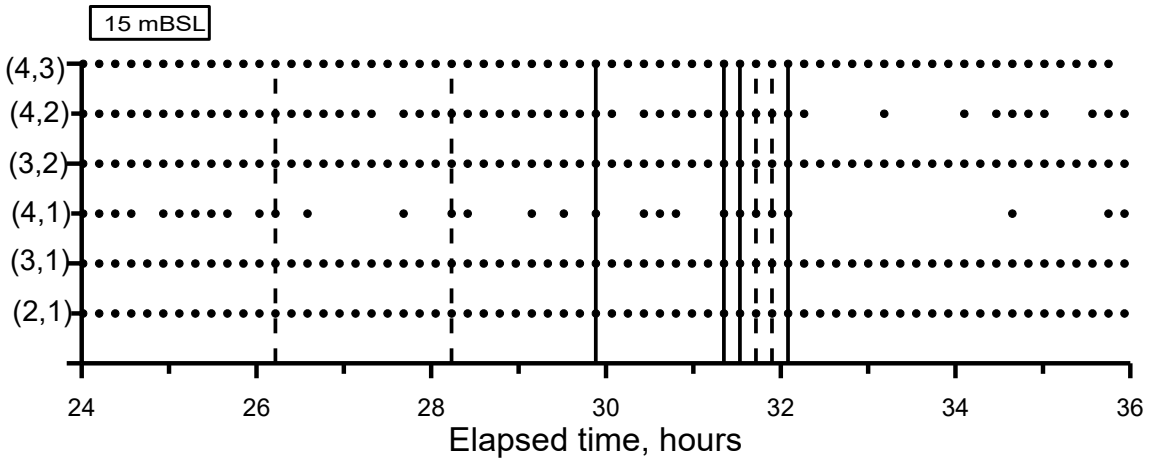

Fig. 7. Time series identifying the existence of 2-channel pseudo-frazil solutions, Frazer et al. data. Solid lines, Group 1, dotted lines Group 2. Elapsed times from1200 (local) November 10 2017.

A total of eight data sets was selected for analysis utilizing the full complement of 2- and 3-frequency solutions. The results fall into two categories, distinguished by the channel pair (2,1) proportional deviations of a^* values with respect to the mean, denoted by Δa^*. The selected data sets, marked on the figure by solid and dotted lines, have Δa^* values of 0.05 and 0.3 for groups 1 and 2 respectively . Figure 8 compares the group averaged deviations for all channel pairs where the anomalous behaviour of the (2,1) pair can clearly be seen.

The strong correlation of individual channel pair deviations across both groups, indicates a systematic mismatch with the pseudo-frazil cross section relationship. In this case, the combination of a largely untried theoretical model, and data collected under challenging

,

environmental conditions complicates the interpretation. The large Δa^* offset for the (2,1) pair is consistent with 20% increase in the Group 2 channel 1 s_V values.

The high deviations of the (2,1) channel pair of Group 2 are then consistent with an elevation of the channel 1 S_V data value, and occupy about 80% of the data stream. The similarity of the offsets of the (3,2), (4,2) and (4,3) channel pairs between the two groups suggest a minor, but consistent mismatch with the backscatter model. This most likely occurs for k_1a_e values associated with channel 3, as channels 1 and 2 lie in the well validated low k_1a_e regime. At the other extreme, the cross section relationship for the channel 4 frequency is self-validated, as it is derived directly from field data via the original bootstrap extension.

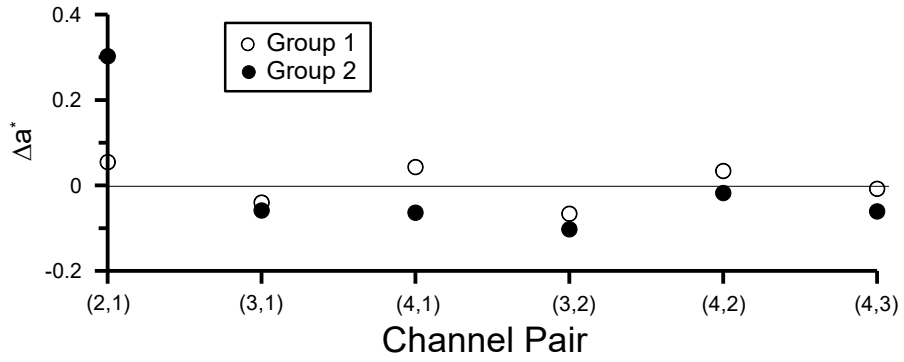

Figure 8. Overall averages of proportional deviations Δ a* for all channel pair combinations.

Table 4shows the full analysis of an example from Group 1, the 15mBSL from Nov. 2017, 11:58 Frazer et al. depth profile with S_V values of -79.7, -72.6, -65.2, and –60.9 dB.

Channel pair	a_m, mm	b	N^*, N	F^*, F	F^*_{Ave}, F_{Ave}	F^*_{Stdev}
(2,1)	0.391	0.000	1981	4.97×10^{-07}	6.46×10^{-07}	7.77×10^{-08}
(3,1)	0.348	0.000	3847	6.82×10^{-07}		
.. (4,1)	0.363	0.000	3040	6.09×10^{-07}		
(3,2)	0.344	0.000	3892	6.66×10^{-07}		
(4,2)	0.366	0.000	2818	5.78×10^{-07}		
(4,3)	0.355	0.000	3779	7.06×10^{-07}		
(3,1)(4,3)	0.338	0.084	4060	6.80×10^{-07}	6.78×10^{-07}	
(3,2)(4,3)	0.329	0.105	4279	6.71×10^{-07}		
(2,1)(3,1)	0.278	0.231	5994	6.83×10^{-07}		
(2,1)(4,2)	-	-	-	-		

Table 4. Fractional volumes for the 15mBSL Nov. 11, 17:58 McMurdo Sound data: pseudo-frazil analysis.

The final result is a 3-frequency fractional volume of $F = 6.78 \times 10^{-7} \pm 7.8 \times 10^{-8}$, ie. an uncertainty of ± 11%, uncharacteristically low compared to the group average of ± 18%.

In contrast, the frazil fractional volume estimates of Frazer et al. (2020), are roughly two orders of magnitude above the pseudo-frazil analysis, similar in magnitude to the Peace River results of Fig. 6, but featuring highly skewed particle distributions. The Frazer et al. (2020) analysis incorporates

,

the 30:1 aspect ratio liquid oblate spheroid model of Kungl et al. (2020). This is in shown with effective radius scaling in Fig. 9, for comparison with the marine converted pseudo-frazil relationship; the bootstrap point on the latter confirms the transfer from fresh to seawater.

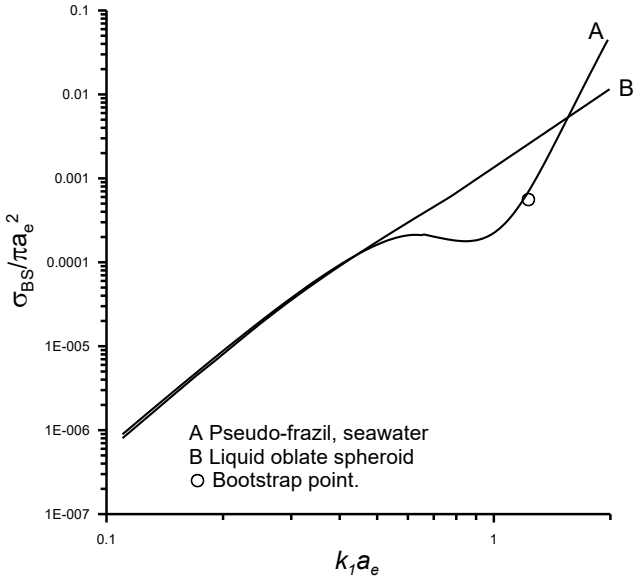

Figure 9. The seawater adapted pseudo-frazil and liquid oblate spheroid backscatter relationships.

The liquid spheroid closely follows the pseudo-frazil relationship up to $k_1 a_e = 0.5$, thereafter resembling the liquid sphere of Fig. 3a, reflecting the absence of shear stress common to liquid models. Where $k_1 a_e < 0.5$, the liquid spheroid supports fully determined solutions for the (2,1)frequency combination alone, which return F^* similar values to the pseudo-frazil analysis; no other solutions could be found. . As our primary interest is in the McMurdo Sound data set is for evaluation of the pseud-frazil algorithm, the Frazer et al. analysis will not be discussed further.

4.0 Summary and conclusions

A semi-empirical backscatter cross section relationship has been developed to allow extraction of parameters quantitatively descriptive of suspension of randomly oriented frazil ice crystals of varying aspect ratio. The resulting generalized cross section relationship, $\sigma_{BS}(k_1 a_e)$, incorporates the "effective-sphere" assumption of Ashton (1983) and is subdivided into two components, the longwave Rayleigh oblate spheroid, and an empirically derived sum of higher order terms. The latter were deduced from 4-frequency acoustic laboratory measurements on neutrally buoyant suspensions of polystyrene spheres and disks which closely matched the geometry of natural frazil ice crystals. The measured backscatter cross sections conformed well to a $\sigma_{BS}(k_1 a_e)$ relationship, irrespective of disk orientation and aspect ratio, confirming the validity of the extended effective sphere scaling. Transfer of the relationship derived from polystyrene/brine suspensions to the freshwater frazil environment utilized the strong similarity of the higher order terms of elastic

,

spheres in the two environments. The transferred relationship was extrapolated to higher k_1a_e values with a "bootstrap" technique utilizing the high frequency channel of the Peace River data.

The final relationship, denoted the "pseudo-frazil" backscatter model was incorporated into an extraction algorithm to return fully determined 3-frequency solutions for a 2-parameter, lognormal particle distribution, for both river and marine frazil ice data. The algorithm defines a relationship between pairs of volume backscatter coefficients sharing a common frequency establishs the existence of fully determined solutions prior to full analysis. Evaluation of data drawn from the Peace River, (Marko et al., 2015) and Antarctic shelf water (Frazer et al., 2020) utilizing both 2- and 3-frequency solutions, gave uncertainties in fractional volume of roughly ± 25%. The high numerical precision of fully determined solutions ensures that estimates of uncertainty reflect the intrinsic properties of the algorithm and data.

At present, the pseudo-frazil relationship is limited in range by the currently limited availability of field data due, in part, to the unreliability of data collected at 235 kHz in the 2011-2012 Peace River study (Marko et al., 2015). Access to data at this frequency and/or additional field measurements can further refine the pseudo-frazil cross section relationship and, in particular, extend it to higher k_1a_e values.

The alternative frazil extraction algorithm based on the liquid oblate spheroid backscatter model proposed by Kungl et al., (2020), cannot in general satisfy the fully-determined condition, and solutions are limited to 2-frequency analysis in the low k_1a_e regime. In general, liquid target-based algorithms are unlikely to be productive in this respect as they cannot reproduce the more complex parameter relationships of scattering by shear sustaining elastic targets.

References

Ashton, G. D., 1983: Frazil ice. In: Theory of Dispersed Multiphase Flow, Academic Press N.Y., 271-289.

Faran, J.J. Jr., 1951: Sound scattering by solid cylinders and spheres. J. Acoust. Soc. 23, pp 405-418.

Frazer, E. K., Langhorne, P. J, Leonard, G. H., Robinson, N.J. and Dániel Schumayer, D. Observations of the size distribution of frazil ice in an ice shelf water plume., 2020. Geophy. Res. Letters, 47, e2020GL090498, https://doi.org/10.1029/2020GL09049.

Ghobrial. T.R., Loewen, M.R. & Hicks, F.E. (2013). Characterizing suspended frazil ice in rivers using upward looking sonars. *Cold Reg. Sci Technol. 86*, 113-126.

Hay, A.E., Schaafsma, A.S., 1989 : Resonance scattering in suspensions. J. Acoust. Soc. 85 (3), 1124-1138,.

Hay, A. E, and J. Sheng, 1992: Vertical profiles of suspended sand concentrations and size from multifrequency acoustic backscatter. J. Geophys. Res. 97 (10), pp 1566-1567.

,

.

Hefner, B. T. and P. L. Marston, 2000: Backscattering enhancements associated with subsonic Rayleigh waves on polymer spheres in water: Observation and modeling for acrylic spheres J. Acoust. Soc. Am. 107, 1930-1936, 2000.

Jasek, M., T. Ghobrial, M. Loewen, F. Hicks, 2011: Comparison of CRISSP1D modeled and SWIPS measured ice concentrations on the Peace River. Proc. 16th Workshop on River Ice. Winnipeg, Man.

Kungl, A. F., D. Schumaye, K. Eamon, A. K. Frazer, P. J. Langhorn, H. Greg, G. H. Leonard, 2020: An oblate spheroidal model for multi-frequency acoustic back-scattering of frazil ice. Cold Reg. Sci Technol, 177, https://doi.org/10.1016/103122.

Marko, J.R., M. Jasek, 2010: Frazil monitoring by multi-frequency shallow water ice profiling (SWIPSA): present state. Proc. IAHR 20th International Symposium on Ice, Lahti, Finland. 12p.

Marko, J. R., D.R. Topham, 2015: Laboratory measurements of acoustic backscattering from polystyrene pseudo- ice particles as a basis for quantitative frazil characterization. *Cold Reg. Sci. Technol. 112*, 66-86.

Marko, J.R., M. Jasek, D.R. Topham, 2015: Multifrequency Analyses of 2011-2012 Peace River SWIPS frazil backscattering data. Cold Reg. Sci. Technol. 110, 102-119.

Marko, J. R. and D. R. Topham, 2021: Analyses of Peace River Shallow Water Ice Profiling Sonar data and their implications for the roles played by frazil ice and in situ anchor ice growth in a freezing river, The Cryosphere, 15, 2473–2489, https://doi.org/10.5194/tc-15-2473-2021, 2021.

Marko, J.R., and D,R Topham: Comments on "Observations of the size of frazil ice in an ice shelf water plume, (Frazer et al., 2020)". In preparation.

McFarlane, V., M. Loewen, F. Hicks, 2017: Measurements of the size distributions of frazil ice particles in three Alberta rivers. Cold Reg. Sci. Technol. 142, pp. 100-117,

Rayleigh, J.W.S., 1897: On the incidence of aerial and electric waves upon small obstacles in the form of ellipsoids or elliptic cylinders and the passage of electric waves through a circular aperture in a conducting screen. Phil. Mag. (5) XLIV, pp28-52. (Scientific Papers volume 4, p 305. Cambridge Library Collections, 1897).

Topham, D.R., 2023: The interpretation of multi-frequency acoustic profiling; Part 1, Exact solutions and their role in the evaluation of acoustic backscatter models